

Stable structures of tantalum at high temperature and high pressure

Yansun Yao^{1,2,*} and Dennis D. Klug³

¹*Department of Physics and Engineering Physics, University of Saskatchewan, Saskatoon, Saskatchewan, Canada, S7N 5E2*

²*Canadian Light Source, Saskatoon, Saskatchewan, Canada, S7N 2V3*

³*National Research Council of Canada, Ottawa, Canada, KIA 0R6*

(Received 22 March 2013; published 5 August 2013)

Knowledge of the structures of Ta that appear at high pressures and high temperatures is critical for addressing the recent controversies regarding the phase diagram and melting temperatures of this refractory metal. Structural searches based on a density functional metadynamics method were therefore employed to obtain candidate structures at high-pressure and finite-temperature conditions. A structural transformation from the initial body-centered cubic phase of Ta stable under ambient conditions to an orthorhombic structure with the space group $Pnma$ is predicted. The $Pnma$ structure is shown to be energetically more favorable and more reasonable than other candidate structures considered previously, since it was also confirmed to be mechanically and dynamically stable by phonon and metadynamics calculations. However, a recently proposed hexagonal- ω phase for dense Ta is found to be mechanically and dynamically unstable when anharmonic effects are characterized by high-temperature, self-consistent phonon calculations.

DOI: [10.1103/PhysRevB.88.054102](https://doi.org/10.1103/PhysRevB.88.054102)

PACS number(s): 81.30.Bx, 62.50.-p, 64.60.My, 71.15.Mb

There is an active discussion in the literature of the structures and properties of elemental Ta. This discussion has been partially due to a controversial set of measurements on the melting temperature of this important refractory metal.¹ The melting temperatures at high pressures of Ta, as obtained in diamond anvil cell (DAC) devices,²⁻⁴ are reported to be roughly a factor of 2 lower than those determined in shockwave (SW) measurements^{5,6} and calculations.^{7,8} Several theories have been developed to explain the large discrepancy in the measured DAC and SW melting curves. For instance, Wu *et al.* suggest that the ambient body-centered cubic (bcc) structure of Ta will undergo a shear-induced phase transition to a partially disordered, partially crystalline structure, along a P - T curve that coincides with the DAC melting curve, before it reaches the true melting curve, the SW melting curve.⁹ However, Burakovsky *et al.* propose that the bcc structure will transform to another ordered structure, the hexagonal- ω (hex- ω) structure, at high temperatures before melting.¹⁰ The hex- ω structure has higher predicted melting temperatures than the bcc structure, which could possibly explain the enhanced melting curve in SW experiments. Despite the difference in details, both theories suggest that dense Ta will likely transform to other polymorphs at high temperatures that can be stabilized via anharmonicity. This hypothesis is partially supported by the shock compression experiments, in which a break in measured sound velocities has been identified before melting, indicating a possible phase transition.⁵ Clearly, accurate knowledge of the structures of Ta at high pressures is critical for understanding the results of both DAC and SW studies in order to reconcile the significant discrepancy.

Recently, the suggestion of the appearance of the hex- ω structure in Ta at high pressure and high temperature has been challenged and is the source of debate.¹¹ Haskins *et al.* suggest that, with the use of combined large-scale molecular dynamics and effective pair potential developed from a model generalized pseudopotential theory, the predicted polymorphism in Ta depends on factors such as size and shape of the simulation cells used in calculations and the

stability of the hex- ω structure suggested in previous studies could be an artifact of insufficient simulation cell size. More importantly, Haskins *et al.* suggests that alternative unknown structures, other than the hex- ω structure, could be used to resolve the question of dense Ta. This indicates a clear need for further examination of this controversy. In this paper, we therefore have investigated the structural evolution of dense Ta by employing the metadynamics method, based on the density functional theory (DFT),¹² which allows structural searches to proceed at high pressures and finite temperatures. We predict a new candidate structure of dense Ta that has lower enthalpies than previously suggested structures, and it is confirmed to be mechanically and dynamically stable. In addition, the mechanical properties and high-temperature stability of the hex- ω structure have been investigated using a self-consistent lattice dynamical method.

Structural optimizations and total energy calculations were performed using the Vienna *Ab initio* Simulation Package (VASP)¹³ and the projector-augmented wave (PAW) potential¹⁴ with the PW91 exchange-correlation functional.¹⁵ The Ta potential employs $5p$, $6s$, and $5d$ as valence states and a kinetic energy cutoff of 290 eV. Dense k -point grids were selected to yield the total energies converged to within 0.5 meV/atom. Specifically, a $16 \times 16 \times 16$ k -point grid was used for the bcc and face-centered cubic (fcc) structures, a $16 \times 16 \times 12$ grid was used for the hexagonal close-packed (hcp) structure, a $16 \times 16 \times 6$ grid was used for the double hexagonal close-packed (dhcp) structure, a $12 \times 12 \times 6$ grid was used for the $Pnma$ structure, a $8 \times 8 \times 16$ grid was used for the hex- ω structure, a $12 \times 12 \times 12$ grid was used for the A15 structure, and a $6 \times 6 \times 12$ grid was used for the β -Ta structure. Temperature-dependent phonons were calculated employing the self-consistent *ab initio* lattice dynamical (SCAILD) method,¹⁶ and results were cross-checked with the ABINIT program (at $T = 0$ K).¹⁷ SCAILD calculations were carried out employing an appropriate size of supercell to yield the phonon frequencies that are converged within 0.05 THz (~ 1.67 cm⁻¹). For the hcp (dhcp), hex- ω , and fcc (bcc)

structures, a supercell of 128, 96, and 64 atoms, respectively, was employed. Because of the ability for investigating anharmonic free-energy surfaces, the first-principles metadynamics method for the study of reconstructive structural transformations in crystals was employed to investigate high pressure–high temperature phase transitions.^{18,19} The metadynamics method was applied and combined with VASP,²⁰ using the same PAW potential and kinetic energy cutoff as described above. The supercells employed in the simulations contain 64 Ta atoms and use a $4 \times 4 \times 4$ k -point grid. Each metastep consists of a first principles molecular dynamics simulation employing a canonical number-volume-temperature (NVT) ensemble, with 400 time steps for a total simulation time of 0.8 ps. This simulation time has been shown to be adequate in previous studies employing the metadynamics method.^{20,21} Gaussian width and height parameters were chosen following the guidelines summarized in Ref. 22. All structures obtained in the metadynamics simulations were verified in carefully converged total energy calculations with the VASP code. The possibility of structures with unit cells larger than 64 atoms was not examined. Mechanical properties were calculated using the Toolkit software employing the VASP code in a symmetry generalized least-square method to obtain elastic coefficients.²³

The metadynamics simulations starting from the initial bcc structure revealed a new structure under high-pressure and high-temperature conditions. The bcc structure was selected as the initial structure, since one needs to begin the structural evolution from a stable configuration (a local or global energy minimum). The hex- ω structure, which has been alternatively suggested, was found to be mechanically and dynamically unstable (see below) and therefore was not employed as an initial structure. In order to accelerate the structural evolution from the initial bcc structure, we compressed and annealed the simulation cell up to 400 GPa and 6000 K. Compressing and heating the system beyond its true transition pressure and temperature may help to decrease the free energy barrier. The new structure [Fig. 1(a)] has a four-atom orthorhombic unit cell with the $Pnma$ space group. The optimized structural parameters for this structure, at 400 GPa, are $4c$ 0.3689, 0.25, and 0.6124 with $a = 4.52$ Å, $b = 3.88$ Å, and $c = 2.26$ Å. The evolution of the $Pnma$ structure from the bcc structure involves two internal constraints: a homogeneous deformation of the $(110)_{bcc}$ planes and a shearing of every second plane along the $[1-10]_{bcc}$ directions [Fig. 1(b) and 1(c)]. This transformation mechanism is similar to the bcc to hcp Burgers path.²⁴ A reason for the preference of this slip system is that the $(110)_{bcc}$ planes have a higher packing density and a greater interplanar separation than other crystallographic planes in a bcc lattice, and this makes their relative displacement easier. In addition, the plane slipping undergoes along a close-packed direction, which results in weaker repulsive force. It is interesting that several elements exhibit or are predicted to have the $Pnma$ space group at high pressure. For instance, Am and Ca have the same space group and similar site symmetries for their component atoms.^{25–27}

To study the microscopic mechanisms for this phase transition, we examined the energy landscape of Ta at 400 GPa [Fig. 1(d)]. The plane deformation shown in the y axis describes a uniform transformation from the $(110)_{bcc}$

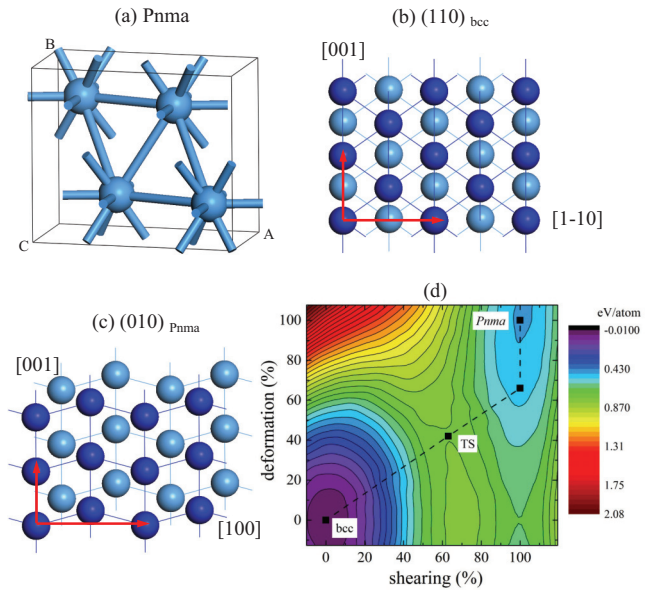


FIG. 1. (Color online) (a) The $Pnma$ structure of Ta. (b) bcc and (c) $Pnma$ structures of Ta viewed along the $[110]_{bcc}$ and $[010]_{pnma}$ directions, respectively. The Ta atoms on different planes are differentiated by using different colors (darkness). (d) Contour plot of the minimized enthalpies of Ta as a function of $(110)_{bcc}$ plane distortion and relative displacement of neighboring planes at 400 GPa. The lowest-energy transition pathway is shown by the dashed lines. At each point, the plane shape and plane displacement were kept fixed, while all other degrees of freedom of the structure were optimized with respect to the trace of stress tensors at 400 GPa.

planes to the $(010)_{pnma}$ planes, during which the atoms move from a body-centered rectangle arrangement into a wavelike modulation. The shearing shown in the x axis corresponds to the relative positions of the planes along the $[1-10]_{bcc}$ direction. Two energy minima are revealed in the lower left and upper right corners of the energy surface, respectively, which correspond to the bcc (no shearing or deformation) and $Pnma$ structure (100% shearing or deformation). The $Pnma$ structure is shown have a local energy minimum in comparison with other candidate structures, which makes it a promising candidate for a metastable phase. As expected, the energy landscape is flatter along the shearing direction than it is for plane deformation. The lowest-energy transition pathway leading from the initial bcc energy well to the neighboring $Pnma$ well is indicated by the dashed lines. This structural transformation consists of two steps. In the first step, a shearing displacement proceeds simultaneously with a plane deformation. While the planes shift along this path direction, the Ta sites on each layer can be maintained above the Ta voids in the neighboring layers, therefore reducing the interplanar repulsive forces. The transition state along this path is shown as a saddle point with the barrier height of ~ 0.6 eV, or ~ 7000 K in terms of temperature, which agrees well with the upper bound temperature (6000 K) used in the metadynamics simulations. In the second step, the configuration approaches toward the $Pnma$ structure through a shallow energy well and proceeds with a plane deformation alone. The nonstationary and saddle points shown in Fig. 1(d)

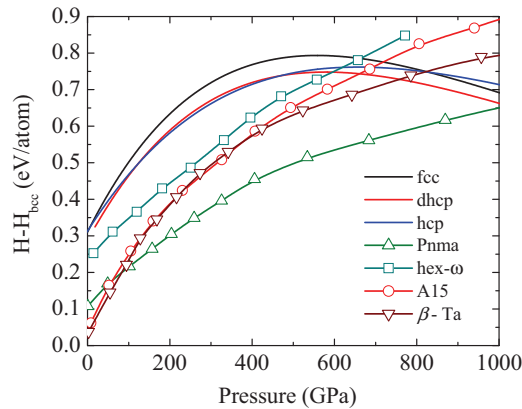


FIG. 2. (Color online) Calculated enthalpies of candidate structures of Ta in the pressure range 0–1 TPa. The enthalpies of the bcc structure are taken as the reference.

are intrinsically unstable, which, if fully relaxed, will yield either the bcc or the *Pnma* structure. Thus, the enthalpies of these points have to be calculated with constraints by fixing one or more structural degrees of freedom.²⁸ Consequently, the calculated energy barrier between the bcc and the *Pnma* structures only represents an upper bound estimate, which is likely an overestimate of the experimental value.

Significantly, the predicted *Pnma* structure is energetically favorable. In Fig. 2, we compare the calculated static enthalpies of the *Pnma* structure, with the experimentally observed structures, and with the structures previously considered as candidates for dense Ta, in a large pressure range from 0 to 1000 GPa (1 TPa). Consistent with previous studies, the bcc structure is the most stable structure at ambient pressure and remains the lowest enthalpy structure over the entire pressure range. In the pressure range, i.e., 50 GPa to 1 TPa, the *Pnma* structure has the lowest enthalpy compared with all other structures. A previously suggested candidate structure for dense Ta, the hex- ω structure,¹⁰ is always less stable than the *Pnma* structure, and its enthalpy becomes increasingly higher than that of the *Pnma* structure at high pressures. The two metastable phases of Ta, the A15 and β -Ta structures, that were previously observed in a supercooled liquid and thin films,^{29,30} are more stable than the *Pnma* structure at ambient pressure and in the low-pressure range. Once the pressure is increased beyond 60 and 83 GPa, respectively, these two structures quickly become less stable than the *Pnma* structure. The relative stabilities of three close-packed candidates, fcc, hcp, and dhcp structures, compared to that of the bcc structure, initially decrease with pressure, but at sufficiently high pressure, they start to increase. Additional enthalpy calculations (not shown) revealed that the fcc, hcp, and dhcp structures have similar enthalpies at pressures beyond 1 TPa and that all three structures become more stable than the bcc structure at sufficiently high pressures.

To investigate the mechanical stability of dense Ta, we calculated the harmonic phonon band structures of the candidate structures over a broad pressure range. The calculated phonon band structures of the fcc, hcp, and dhcp structures reveal imaginary frequencies in the Brillouin zone at 1 bar, indicating they are unstable phases. However, the bcc and A15

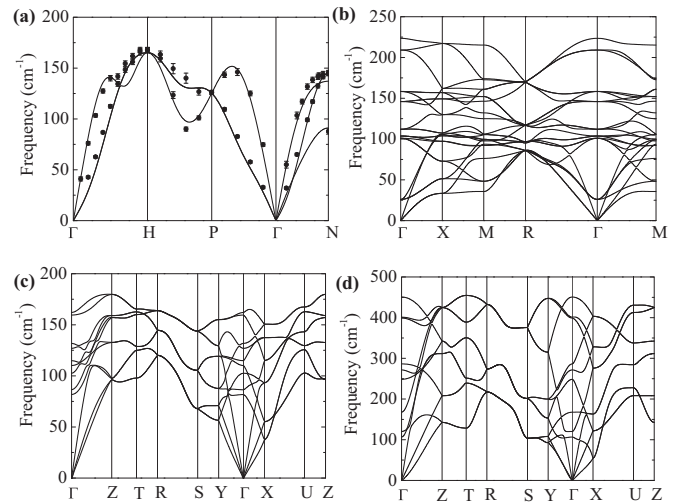


FIG. 3. Harmonic ($T = 0$ K) phonon band structures of (a) bcc and (b) A15 structures calculated at 1 bar. Symbols with error bars in (a) are experimental data from Ref. 31. Harmonic phonon band structures of the *Pnma* structure calculated at (c) 1 bar and (d) 400 GPa.

structures were found to be mechanically stable from 1 bar to at least 1 TPa. In Fig. 3(a) and 3(b), harmonic phonon band structures for the bcc and A15 structures calculated at 1 bar are shown. The theoretical phonon band structure for the bcc structure shows a good agreement with the ambient experimental data.³¹ The bcc phonons exhibit a frequency range from 0 to ~ 170 cm^{-1} . In comparison, the A15 phonons have an extended frequency range to ~ 225 cm^{-1} . Higher vibrational frequencies in the A15 structure originate from the motions of the Ta pairs located on each faces of the cubic unit cell, which form linear chains along cubic axes. The Ta-Ta spacing in these linear chains is 2.65 \AA at 1 bar, which is significantly shorter than the shortest Ta-Ta distance in the bcc structure (2.87 \AA).

The *Pnma* structure is mechanically stable from 1 bar to at least 400 GPa without showing imaginary frequencies [Fig. 3(c) and 3(d)]. At 1 bar, the *Pnma* structure has a range of phonon frequencies similar to that of the bcc structure, indicating that these two structures contain similar vibration modes. Indeed, as discussed earlier, the bcc and *Pnma* structures have some resemblances in their structural motifs. At 1 bar, the closest Ta-Ta distances in the *Pnma* structure are between 2.84 and ~ 2.88 \AA , which compares well with that of the bcc structure. While their phonon frequencies cover a similar range, the detailed distributions of the phonons appear to be different in the bcc and the *Pnma* structures (Fig. 4). Compared with the bcc phonons, the *Pnma* phonons carry more weight in the low-frequency range. Lower-frequency phonons are easier to excite and therefore contribute more effectively to the entropy. Thus, at finite temperatures, the vibrational free energy for the *Pnma* structure would be slightly lower than that of the bcc structure. As an example, we employed a quasiharmonic approximation,³² from which we estimated that at $P = 400$ GPa and $T = 6000$ K, the vibrational free energy and vibrational entropy of the bcc structure are -4.284 eV/atom and 0.973 meV K^{-1} /atom,

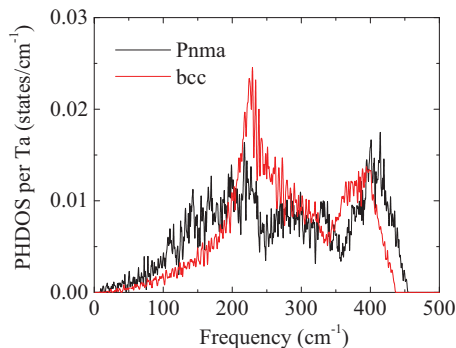


FIG. 4. (Color online) Calculated phonon density of states (PHDOS) for the bcc and the *Pnma* structures at 400 GPa.

respectively. At the same P - T condition, the vibrational free energy and vibrational entropy of the *Pnma* structure were calculated to be -4.386 eV/atom and 0.989 meV K^{-1} /atom, respectively. At 400 GPa, the calculated enthalpies for the bcc and the *Pnma* structures are 19.096 and 19.535 eV/atom, respectively (see Fig. 2). Thus, at finite temperatures, the energy differences between the bcc and *Pnma* structures are likely being reduced from the values calculated at 0 K due to the phonon contributions.

In principle, the temperature-dependent phonon dispersion relations and vibrational free energy of the Ta polymorphs can be calculated employing the SCAILD method, which treats explicitly the phonon-phonon interactions and anharmonic effects that may arise in Ta at finite temperatures. In the next paragraph, we explain in detail the temperature-dependent phonon band structures of the hex- ω structure derived from the SCAILD method. Compared with the hex- ω structure, however, the *Pnma* structure has lower symmetry and a larger unit cell; therefore, the SCAILD calculation of the *Pnma* structure is more computationally demanding. Convergence tests showed that the phonon band structure of the *Pnma* structure requires a supercell with a size of at least 144 atoms ($3 \times 3 \times 4$), and the force calculations at finite temperatures may need several tens of distortion steps to converge. Thus, we do not provide a direct evaluation of the SCAILD phonon band structure for the *Pnma* structure, but its stabilities at finite temperatures can be inferred from the metadynamics simulations. Moreover, a detailed phase diagram and the melting lines of the *Pnma* structure can be determined, for example, following the first principles approaches described in Ref. 11. The pressure and temperature of the bcc-*Pnma*-liquid triple point can also be determined by computing the bcc and *Pnma* melting curves and locating their intersection point. However, these calculations are beyond the scope of the present paper.

One of the current controversies about dense Ta is whether the hex- ω structure is a valid candidate for the high-temperature polymorphs. In our harmonic phonon calculations, the hex- ω structure exhibits imaginary vibrational frequencies over the entire pressure range considered, extending from 1 bar to 1 TPa. Figure 5(a) shows the harmonic phonon band structure of the hex- ω structure calculated at 1 bar (solid curves), as seen when the imaginary frequencies go below $100i$ cm^{-1} . The ratios of the c -axis lengths to the a -axis lengths, c/a , employed for these calculations were obtained

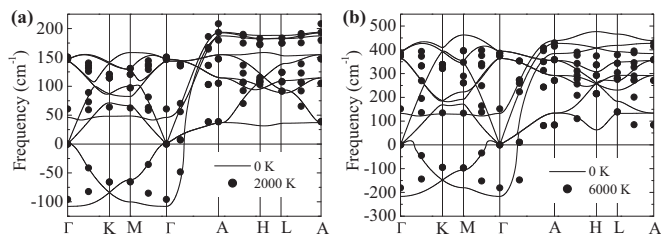


FIG. 5. Harmonic ($T = 0$ K) and anharmonic ($T > 0$ K) phonon band structures of the hex- ω structure calculated at (a) 1 bar and (b) 400 GPa.

from the DFT structural optimizations. The optimized c/a ratio increases slowly from the ambient pressure value of ~ 0.56 to ~ 0.58 at 500 GPa, which is in good agreement with the values obtained in Refs. 10 and 11. In order to investigate the high-temperature stability of the hex- ω structure, we employed the SCAILD method¹⁶ that permits a DFT calculation of the first principles phonons and free energies as a function of temperature. The SCAILD method is conceptually similar to

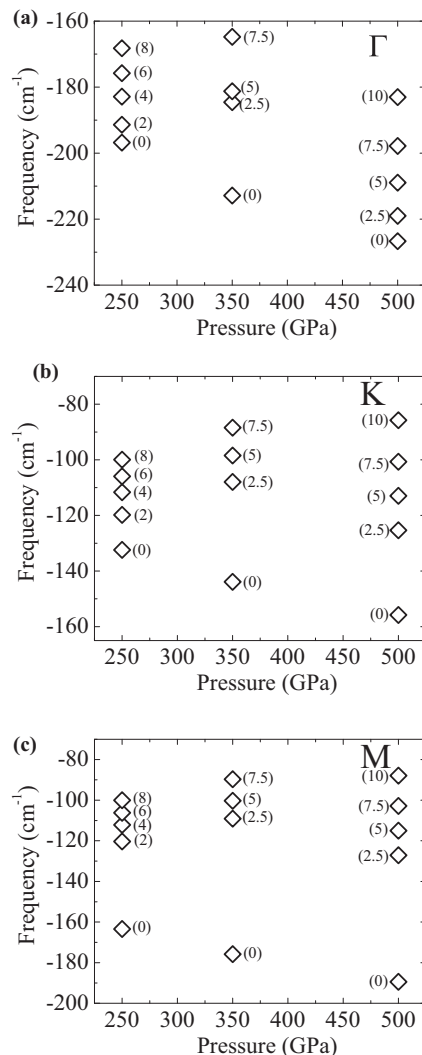


FIG. 6. Evolution of the imaginary phonon frequencies with pressure and temperature at (a) Γ , (b) K , and (c) M points. Numbers in brackets are temperatures in units of 1000 K.

the renormalized harmonic approximation, which incorporates the anharmonic effects through the temperature dependence of phonon frequencies, taking account of phonon-phonon interactions. In Fig. 5(a), the SCAILD corrected phonon frequencies at 2000 K are shown in solid dots, which indicate somewhat enhanced frequencies from $T = 0$ K, along with the appearance of phonon degeneracies at the K , M , and L symmetry points. We repeated the harmonic and SCAILD phonon calculations at 400 GPa and $T = 6000$ K but observed no sign of increased instability [Fig. 5(b)]. We then extended the temperature-dependent phonon calculations of the hex- ω structure to higher pressures up to 1 TPa, and to higher temperatures up to the melting line, but did not find that the hex- ω structure becomes stable. Figure 6(a)–6(c) shows the evolutions of the imaginary phonon frequencies at the Γ , K , and M points of the hex- ω structure at different pressures and temperature. Several temperatures were chosen below the melting line at each pressure. It is therefore interesting that previously suggested hex- ω structure is predicted not to be stable near the melting temperature within the anharmonic theory considered here.

The elastic moduli of the $Pnma$ structure were calculated, together with its compressibility and sound velocities, for comparison of these properties with the bcc and A15 structures. The bcc elastic moduli calculated with PAW pseudopotentials employing $5p$, $6s$, and $5d$ as valence states yielded values in good agreement with the C_{11} , C_{12} , and C_{44} elastic constants and shear modulus reported in Refs. 33 and 34. The main difference between the present calculations and those of Refs. 33 and 34 is the use of the PAW potential in a density functional treatment. The bulk modulus of the bcc, A15, and $Pnma$ structures are all calculated to be within a 3% range of ~ 1471 GPa at a pressure of 400 GPa. At 400 GPa, the C_{11} elastic constant for the $Pnma$ structure is calculated to be 1862 GPa compared with 1877 GPa for the bcc structure at 412 GPa of Ta. The other elastic constants for the $Pnma$ structure at 400 GPa are $C_{12} = 1420$ GPa, $C_{13} = 1126$ GPa, $C_{22} = 1906$ GPa,

$C_{23} = 1000$ GPa, $C_{33} = 2214$ GPa, $C_{44} = 210$ GPa, $C_{55} = 82$ GPa, and $C_{66} = 234$ GPa. The C_{12} and C_{44} elastic constants for the bcc structure at 400 GPa are 1305 and 392 GPa, respectively. The shear modulus obtained within the Voigt criteria³⁵ for the $Pnma$ structure is 268 GPa compared with 350 GPa for the bcc Ta at 400 GPa. The lower shear modulus for the $Pnma$ structure than that of the bcc structure appears to be consistent with the deviation from the 90° angles of nearest neighbors in the $Pnma$ structure in comparison with the perfect 90° near-neighbor angles in the bcc structure. The deviation from 90° in the $Pnma$ structure may suggest a more strained metallic bonding that contributes to a lower shear modulus. This could also be tested since the elastic properties could, in principle, be measured since the $Pnma$ structure may be quench recoverable.

In summary, we have predicted a new $Pnma$ structure as a high-pressure–high-temperature form of Ta using the metadynamics structural search method. It is found that the $Pnma$ structure obtained via metadynamics simulations is both dynamically and mechanically stable at 0 K and high temperatures, while it is also energetically favorable at high pressures. A mechanism for the transformation from the initial bcc structure to the $Pnma$ structure has been characterized. A previously suggested candidate structure for dense Ta, the hex- ω structure, is found to be energetically unfavorable and mechanically unstable.

Y.Y. gratefully acknowledge the Information and Communications Technology group at the University of Saskatchewan for providing computing resources, the Socrates cluster and the Plato cluster, which are part of the High Performance Computing Training and Research Facilities at the University of Saskatchewan. Some of the calculations were performed using computing resources provided by WestGrid and Compute Canada. This project was supported by a Natural Sciences and Engineering Research Council of Canada Discovery Grant.

*Corresponding author: yansun.yao@usask.ca

¹D. D. Klug, *Physics* **3**, 52 (2010).

²D. Errandonea, B. Schwager, R. Ditz, C. Gessmann, R. Boehler, and M. Ross, *Phys. Rev. B* **63**, 132104 (2001).

³D. Errandonea, M. Somayazulu, D. Häusermann, and H. K. Mao, *J. Phys.: Condens. Matter* **15**, 7635 (2003).

⁴A. Dewaele, M. Mezouar, N. Guignot, and P. Loubeyre, *Phys. Rev. Lett.* **104**, 255701 (2010).

⁵J. M. Brown and J. W. Shaner, in *Shock Waves in Condensed Matter—1983*, edited by J. Asay, R. A. Graham, and G. K. Straub (North-Holland, Amsterdam, 1984), p. 91.

⁶C. Dai, J. Hu, and H. Tan, *J. Appl. Phys.* **106**, 043519 (2009).

⁷S. Taioli, C. Cazorla, M. J. Gillan, and D. Alfè, *Phys. Rev. B* **75**, 214103 (2007).

⁸Z.-L. Liu, L.-C. Cai, X.-R. Chen, and F.-Q. Jing, *Phys. Rev. B* **77**, 024103 (2008).

⁹C. J. Wu, P. Söderlind, J. N. Glosli, and J. E. Klepeis, *Nat. Mater.* **8**, 223 (2009).

¹⁰L. Burakovsky, S. P. Chen, D. L. Preston, A. B. Belonoshko, A. Rosengren, A. S. Mikhaylushkin, S. I. Simak, and J. A. Moriarty, *Phys. Rev. Lett.* **104**, 255702 (2010).

¹¹J. B. Haskins, J. A. Moriarty, and R. Q. Hood, *Phys. Rev. B* **86**, 224104 (2012).

¹²W. Kohn and L. J. Sham, *Phys. Rev.* **140**, A1133 (1965).

¹³G. Kresse and J. Hafner, *Phys. Rev. B* **47**, 558 (1993).

¹⁴G. Kresse and D. Joubert, *Phys. Rev. B* **59**, 1758 (1999).

¹⁵J. P. Perdew and Y. Wang, *Phys. Rev. B* **45**, 13244 (1992).

¹⁶P. Souvatzis, O. Eriksson, M. I. Katsnelson, and S.P. Rudin, *Comput. Mater. Sci.* **44**, 888 (2009).

¹⁷X. Gonze, J.-M. Beuken, R. Caracas, F. Detraux, M. Fuchs, G.-M. Rignanese, L. Sindic, M. Verstraete, G. Zerah, F. Jollet, M. Torrent, A. Roy, M. Mikami, Ph. Ghosez, J.-Y. Raty, and D. C. Allan, *Comput. Mater. Sci.* **25**, 478 (2002).

¹⁸R. Martoňák, A. Laio, and M. Parrinello, *Phys. Rev. Lett.* **90**, 075503 (2003).

¹⁹R. Martoňák, D. Donadio, A. R. Oganov, and M. Parrinello, *Nat. Mater.* **5**, 623 (2006).

- ²⁰Y. Yao and D. D. Klug, *Phys. Rev. B* **85**, 214122 (2012).
- ²¹Y. Yao, D. D. Klug, R. Martoňák, and S. Patchkovskii, *Phys. Rev. B* **83**, 214105 (2011).
- ²²R. Martoňák, *Eur. Phys. J. B* **79**, 241 (2011).
- ²³Y. Le Page and P. Saxe, *Phys. Rev. B* **65**, 104104 (2002).
- ²⁴W. G. Burgers, *Physica (Amsterdam)* **1**, 561 (1934).
- ²⁵S. Heathman, R. G. Haire, T. Le Bihan, A. Lindbaum, K. Litfin, Y. Méresse, and H. Libotte, *Phys. Rev. Lett.* **85**, 2961 (2000).
- ²⁶Y. Yao, J. S. Tse, Z. Song, D. D. Klug, J. Sun, and Y. Le Page, *Phys. Rev. B* **78**, 054506 (2008).
- ²⁷Y. Nakamoto, M. Sakata, K. Shimizu, H. Fujihisa, T. Matsuoka, Y. Ohishi, and T. Kikegawa, *Phys. Rev. B* **81**, 140106(R) (2010).
- ²⁸H. T. Stokes and D. M. Hatch, *Phys. Rev. B* **65**, 144114 (2002).
- ²⁹L. Cortella, B. Vinet, P. J. Desre, A. Pasturel, A. T. Paxton, and M. van Schilfgaarde, *Phys. Rev. Lett.* **70**, 1469 (1993).
- ³⁰S. L. Lee, M. Doxbeck, J. Mueller, M. Cipollo, and P. Cote, *Surf. Coat. Technol.* **177–178**, 44 (2003).
- ³¹A. D. B. Woods, *Phys. Rev.* **136**, A781 (1964).
- ³²P. Pavone, S. Baroni, and S. de Gironcoli, *Phys. Rev. B* **57**, 10421 (1998).
- ³³O. Gülseren and R. E. Cohen, *Phys. Rev. B* **65**, 064103 (2002).
- ³⁴M. Foata-Prestavoine, G. Robert, M.-H. Nadal, and S. Bernard, *Phys. Rev. B* **76**, 104104 (2007).
- ³⁵O. L. Anderson, *J. Phys. Chem. Solid.* **24**, 909 (1963).